WORLD CONFERENCE ON TIMBER ENGINEERING 2025
BRISBANE, AUSTRALIA
Advancing Timber for the Future Built Environment

PERFORMANCE BASED DESIGN METHOD FOR TIMBER UNIT LOAD-BEARING WALL COMPOSED OF CURVED MEMBERS CONSIDERING GEOMETRIC NONLINEARITY AND PERFORMANCE OF JOINTS

Shion KUBOTA[1], Ayumu YASUI[2], Shinta YOSHITOMI[3]

ABSTRACT: This study proposes a load-bearing wall system composed of curved wooden member units, allowing designers to freely control stiffness and strength. This system allows for independent control of stiffness and strength by adjusting the unit size, sectional dimensions, or curvature. In addition, a performance-based design method is proposed by solving an inverse problem that enables to change the appearance without affecting the performance. This system can be used as a load-bearing wall for various types of structures, such as old traditional wooden buildings with low stiffness and strength but high deformation performance. A deatailed model is proposed to estimate the stiffness and strength of the unit system by concidering geometric nonlinearity of curved member and the performance of joints. The validity of the proposed method is examined by comparing experimental results with analytical results.

KEYWORDS: load-bearing wall, inverse problem, performance design, curved member

1 – INTRODUCTION

In Japan, traditional wooden houses are commonly reinforced with seismic elements such as braces and load-bearing walls. However, in timber structures with high deformation capacity, i.e. Japanese wooden houses, installing high-stiffness braces can sometimes cause damage to the joints. This study proposed a new load-bearing wall composed of curved members, which not only improve the appearance but also enable the designers to independently control its structural performance and appearance.

Previous research [1] proposed a load-bearing wall system composed of curved member units, enabling separate control of structural performance and appearance (Fig. 1). This approach establishes a relationship between the shape of an individual curved member and its stiffness and strength, formulating an equation to evaluate the overall performance of a load-bearing wall composed of multiple units. By applying back-calculation using this equation, the method identifies the optimal member shape corresponding to a given stiffness and strength. However, previous studies have not concidered for geometric nonlinearity or joint details. Therefore, this study extends the previous method by concidering these factors. In order to examine the effect of these factors, numerical analysis results and experimental data are compared. The curved members are constructed from cutting plywood, and material tests are conducted to clarify its anisotropic properties.

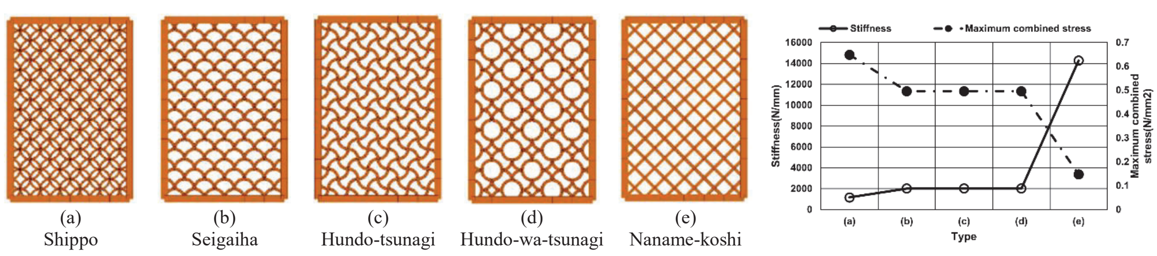

Figure 1. Performance Analysis of Japanese Traditional Patterned Bearing Wall

[1] Shion KUBOTA, Graduate School of Science and Engineering, Ritsumeikan University, Kusatsu, Japan, ru0106kp@ed.ritsumei.ac.jp

[2] Ayumu YASUI, Graduate School of Engineering, Osaka University, Osaka, Japan

[3] Shinta YOSHITOMI, College of Science and Engineering, Ritsumeikan University, Kusatsu, Japan, yositomi@fc.ritsumei.ac.jp

https://doi.org/10.52202/080513-0236

2 – MATERIAL TESTS OF PLYWOOD

2.1 METHOD

Bending, compression, shear, and embedment tests are conducted on specimens cut from 12 mm thick Lauan plywood, with the fiber direction varying from 0° to 90° in 15° increments (Fig. 2). The fiber direction of the plywood surface is aligned with the axial force direction of the member at 0°, and three specimens are prepared for each fiber direction. The specimens for the bending, compression, shear, and embedment tests are made by bonding four sheets of plywood together using woodworking adhesive. In the bending test, a strain gauges are attached to the tensile side at the center of the specimens. In the embedment test, a semicircular groove with a diameter of 12 mm is hollowed out from the specimens, and a drift pin of the same diameter is embedded into the groove.

Bending strength F_b [N/mm^2], Young's modulus E_w [N/mm^2], compressive strength F_c [N/mm^2], tensile strength F_t [N/ mm^2], shear strength F_s [N/ mm^2], embedment strength F_e [N/ mm^2], and embedment stiffness K_e [N/ mm^2] were calculated using equation (1) to (6) based on load F [N], maximum load F_{ult} [N], displacement δ [mm], strain ε, section modulus Z [mm3], cross-sectional area A [mm^2], depth b [mm], and fastener diameter d [mm].

$$F_b = 6dF_{ult}/2Z = 3dF_{ult}/Z \quad (1)$$

$$E_w = F_b/\varepsilon \quad (2)$$

$$F_c = F_t = F_{ult}/A \quad (3)$$

$$F_s = 3F_{ult}/4A \quad (4)$$

$$F_e = F_{ult}/bd \quad (5)$$

$$K_e = F/\delta \quad (6)$$

2.2 RESULTS

Fig. 3 represents the load-deformation relationships at fiber directions of 0°, 45°, and 90° for each test, with one example shown for clarity. Fig. 4 displays the averages of the various strengths, Young's modulus, and embedment stiffness for each fiber direction. In the bending test at 0°, due to the setup cause the center of the specimen to touch the ground before failure; therefore, the maximum load is estimated from its stiffness. The result of the first specimen in the compression test at 0° is excluded from the average calculation of compressive strength because it breaks under less than half the load of the other two specimens. The embedment strength was determined based on the maximum load measured within the displacement range of up to 8 mm, where the drift pin was adequately embedded.

In the bending, compression, tensile, and shear tests, the strength tends to be lowest when the fiber direction is at 45°. On the other hand, no such trend is observed in the embedment test. In particular, the embedment stiffness results are inconsistent even within the same fiber direction.

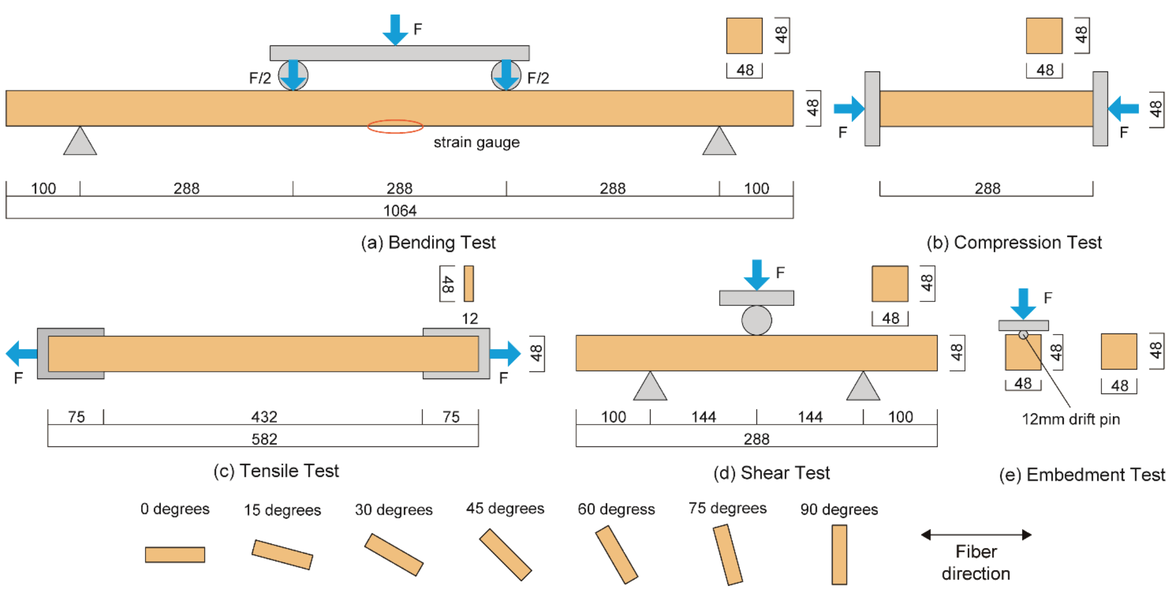

Figure 2. Material Test Method

https://doi.org/10.52202/080513-0236

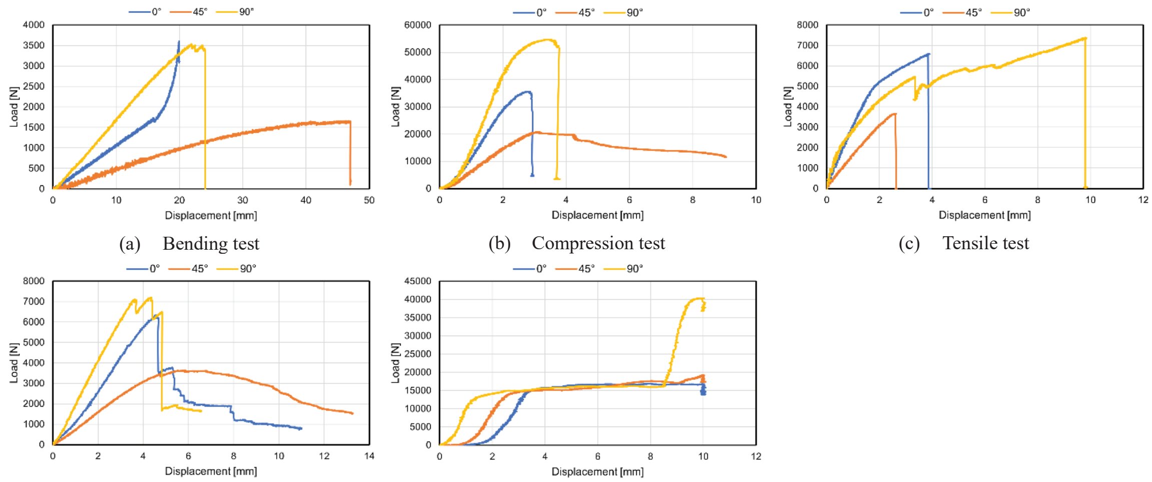

(a) Bending test (b) Compression test (c) Tensile test

(d) Shear test (e) Embedment test

Figure 3. Load-Deformation Curve of Material Test

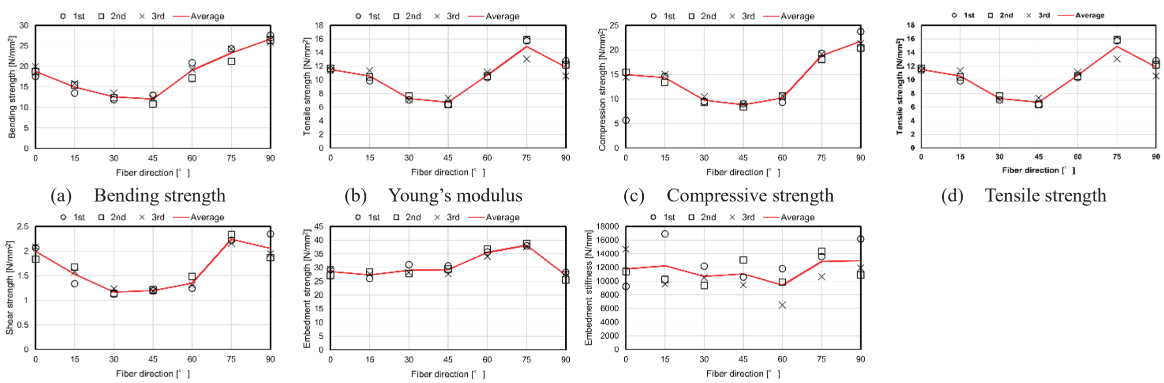

(a) Bending strength (b) Young's modulus (c) Compressive strength (d) Tensile strength

(e) Shear strength (f) Embedment strength (g) Embedment stiffness

Figure 4. Comparison of Structural Performance Based on Fiber Direction Differences

3 – DESIGN METHOD

3.1 GEOMETRIC NONLINEARITY OF CURVED MEMBER UNIT

As shown in Fig. 5, a curved member with a unit size a [mm], radius r [mm], central angle φ [rad], effective width b [mm], and visible width h [mm] is assumed to be installed diagonally across a lattice and subjected to a horizontal load P [N]. The stresses acting on the curved members are defined as axial force $N(\theta)$, shear force $Q(\theta)$, and bending moment $M(\theta)$. Let $\delta_{(1)}$ denote the initial deformation at the center of the curved member unit.

Fig. 6 shows that the curved member unit is divided into three components: steel plates, joint sections, and a plywood member. The initial deformation also can be expressed as the sum of the deformations due to steel plate $\delta_{s(1)}$, joint section $\delta_{r(1)}$, and plywood $\delta_{w(1)}$ as in equation (7). Deformations due to the steel plate and plywood are calculated using the virtual work method. The deformation due to joints are considered as deformation due to joint rotation.

$$\delta_{(1)} = \delta_{s1} + \delta_{r1} + \delta_{w1} \tag{7}$$

To account for geometric nonlinearity, the additional moment generated by the initial deformation $\delta_{(1)}$ is incorporated into the bending moment, and the deformation is recalculated iteratively. The deformation at the n-th step of the iterative calculation, $\delta_{(n)}$, can be expressed using equation (8). As a result, the deformation that includes the effects of geometric nonlinearity $\delta_{(\infty)}$ can be expressed using the coefficient c, as shown in equation (9). A detailed derivation of the equations is presented in the appendix.

$$\delta_{(n)} = \left(1 - c^{n}\right)\delta_{(1)} \big/ (1 - c) \tag{8}$$

$$\delta_{(\infty)} = \lim_{n\to\infty} \delta_{(n)} = \delta_{(1)} \big/ (1 - c) \tag{9}$$

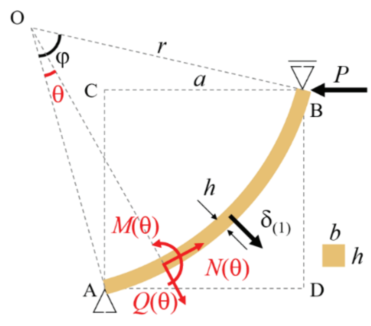

Figure 5. Model of Curved Member Unit

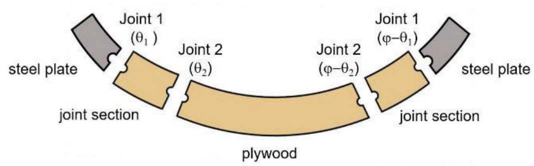

Figure 6. Composition of Curved Members

3.2 CALCURATION OF FAILURE LOAD AND STIFFNESS

The horizontal loads at which edge stress due to axial force and bending moment σ(φ/2) [N], tensile failure P_t [N], shear failure P_s [N], and embedment failure P_e [N] occur in the curved member are calculated, and the minimum among these loads is defined as the strength of the curved member. Each failure load is determined by equation (10) to (13). Bending failure is assumed to occur at the center of the member, while other failures are assumed to occur at joint 2. The stiffness of one unit k [N/mm] is based on the equation from previous research [1] and expressed as follows equation (14). Let the distance between joints be r_{12} [mm]. Detailed derivations of each equation are presented in the appendix.

$$\sigma(\varphi/2) = F_b = \left|M(\varphi/2)\right|/Z + \left|N(\varphi/2)\right|/A \quad (10)$$

$$P_u = b(h-d)F_y = N(\theta_2) \quad (11)$$

$$P_{uw} = b(h-d)F_s = M(\theta_2)/r_{12} \quad (12)$$

$$P_{uj} = bdF_e = M(\theta_2)/r_{12} \quad (13)$$

$$k = \frac{E_w A I_w}{rI(\sin\varphi + \varphi) + r^3 A\{-3\sin\varphi + (2+\cos\varphi)\varphi\}} \quad (14)$$

3.3 INVERSE PROBLEM-BACED DESIGN

Among the five parameters—effective width b, visible width h, central angle φ, stiffness K, and strength P—any three parameters are specified to determine the remaining two unknown parameters. In contrast, inverse problem expressed by equation (15) is formulated by reversing the known and unknown quantities, allowing the effective width and visible width to be determined based on a given central angle, stiffness $\overline{K}$, and strength $\overline{P}$.

$$\begin{gathered}\text{Find } b,\ h \\ \text{Subject to } K = \overline{K}, P = \overline{P}\end{gathered} \quad (15)$$

In this case, the problem involves finding the unknown visible and effective widths that minimize the sum of squared errors e, expressed in equation (16), aligning the target stiffness and strength with the predicted values. Therefore, a numerical solution using a general minimization algorithm can be applied.

$$\begin{gathered}\text{Find } b,\ h \\ \text{To minimize } e = \left\{\left(K-\overline{K}\right)/\overline{K}\right\}^2 + \left\{\left(P-\overline{P}\right)/\overline{P}\right\}^2\end{gathered} \quad (16)$$

4 –EXPERIMENTAL TEST OF TIMBER CURVED MEMBER UNIT

4.1 METHOD

Fig. 7 shows the experimental setup. As shown in Table 1 and Fig. 8, three specimens are created for the linear and curved members with central angles of 30°, 60°, and 90°. These specimens are constructed by bonding four 12 mm-thick sheets and one 5.5 mm-thick sheet of Lauan plywood using woodworking adhesive. A steel plate is inserted into a slit in the middle of the layer, and four 12 mm diameter drift pins are driven in to secure the plywood. The steel plate has 13 mm diameter holes for inserting drift pins. The specimens ware positioned vertically, with pin connections at both ends.

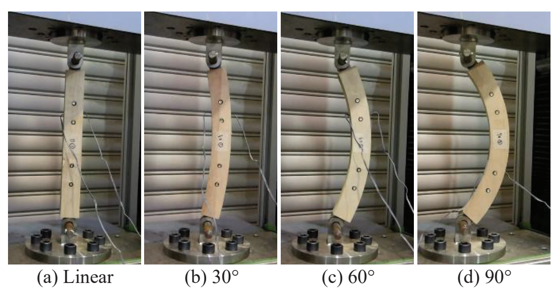

Figure 7. Experimental setup

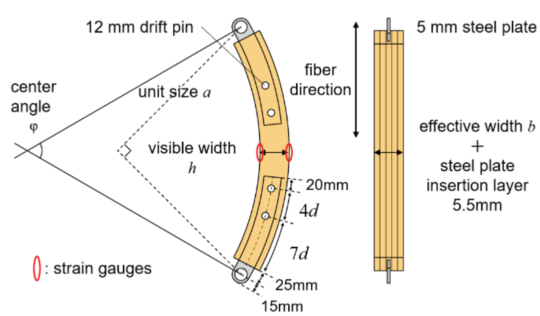

Figure 8. Specimen Diagram

https://doi.org/10.52202/080513-0236

Loading is applied in two cycles of positive and negative within the interlayer deformation angle range of 1/200 rad to 1/15 rad (Table 2). This cycle is assumed to cause deformation in the members arranged along the diagonal of the lattice (Fig. 9).

4.2 RESULTS

The load-deformation curves for each specimen are shown in Fig. 10. The positive side experienced tension, while the negative side underwent compression. Due to a 1 mm clearance in the holes of the steel plate, a slip of approximately 2 to 3 mm is observed near the origin on both the positive and negative sides; however, no additional slip occurred once the load began to take effect. All three linear members fails at joint 2 during tension, which corresponds to the fact that their tensile strength is lower than their compressive strength. In contrast, the failure modes of the curved members varied regardless of the central angle, displaying three patterns: bending failure at the center, failure at joint 2, and mixture of both pattern (Fig. 11).

Table 1: Timber Unit Settings

	(a) Linear	(b) 30°	(c) 60°	(d) 90°
Central angle [°]	–	30	60	90
Unit size [mm]	300			
Effective width [mm]	48			
Visible width [mm]	48			

Table 2: Loading Cycle

Interlayer deformation angle [rad]	1/200	1/150	1/100	1/75	1/50	1/30	1/15
Displacement [mm]	1.06	1.41	2.12	2.83	4.24	7.07	14.14

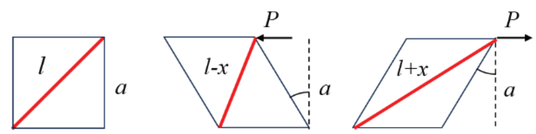

(a) Unloaded state (b) Under commpression (c) Under tension

Figure 9. Deformation Diagram of Unit

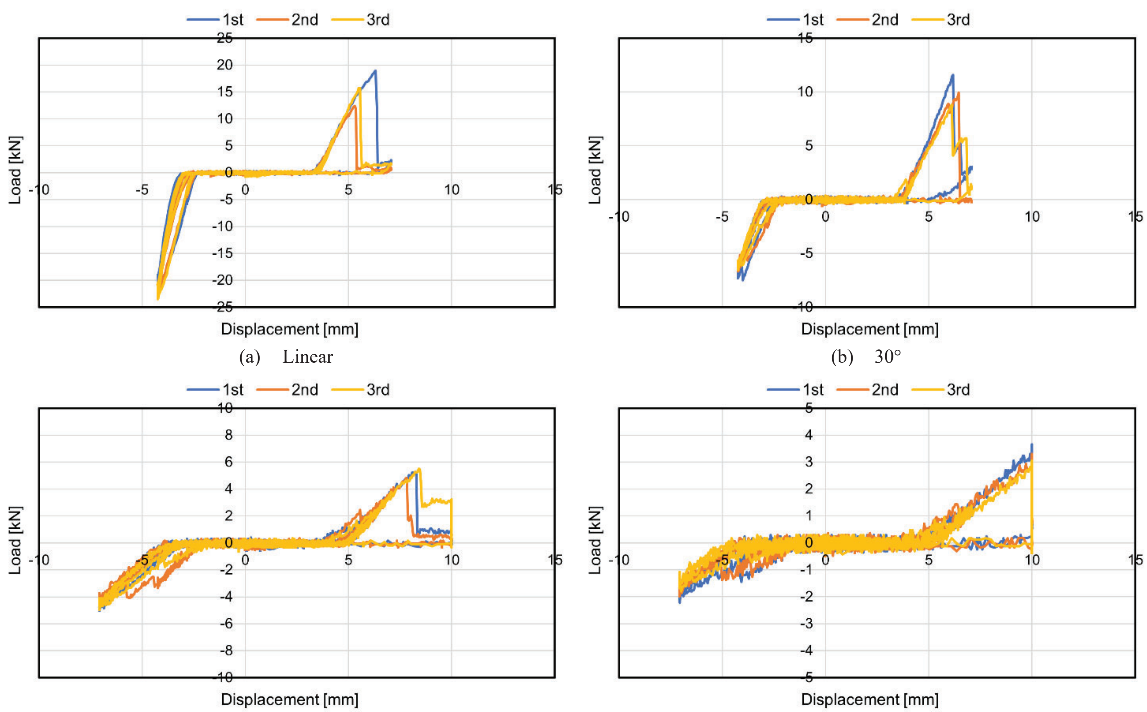

(a) Linear

(b) 30°

(c) 60°

(d) 90°

Figure 10. Load-Deformation Curve of Unit Experiment

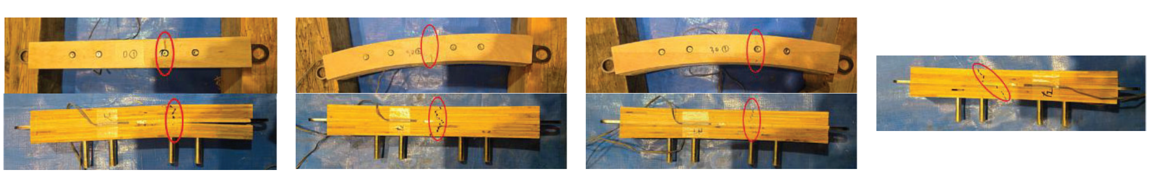

(a) Linear member Failure at joint 2

(b) Curbe member pattern 1 Bending failure at the center

(c) Curbe member pattern 2 Failure at joint 2

(d) Curbe member pattern 3 Mixture of both pattern 1 & 2

Figure 11. Failure Pattern of Unit

5 – VERIFICATION OF THE DESIGN METHOD

5.1 STRENGTH OF THE TIMBER UNIT

Fig. 12 illustrates the relationship between the fiber direction θ_φ [deg] and the position of the curbed member unit. The fiber direction in the curved member is set to be 0° at the center. The fiber direction at an angle θ is given by equation (17). As shown in the equation, this angle also varies depending on the central angle of the curved member.

$$\theta_\varphi = \varphi/2 - \theta \tag{17}$$

The values for compressive strength, tensile strength, shear strength, embedment strength, and embedment stiffness of plywood were taken at the location of joint 2. The bending strength and Young's modulus were standardized to the values at the center of the unit. The results of each strength and stiffness are summarized in Table 3.

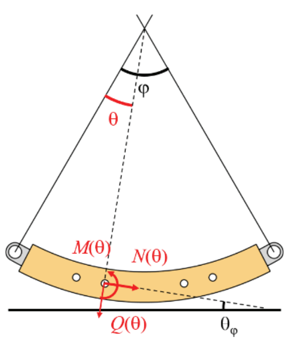

Figure 12. Relationship between Fiber Direction and Curve

Table 3: Structural Performance of Each Specimens

	(a) Linear	(b) 30°	(c) 60°	(d) 90°
Bending strength [N/mm^2]	18.77			
Young's modulus	4466			
Compressive strength [N/mm^2]	14.95	14.75	14.55	14.35
Tensile strength [N/mm^2]	11.53	11.21	10.88	10.55
Shear strength [N/mm^2]	1/99	1.84	1.68	1.53
Embedment strength [N/mm^2]	28.56	30.85	34.49	38.12

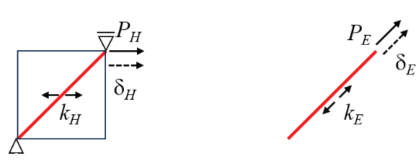

(a) In calculation (b) In experiment

Figure 13. Deformation Diagram

5.2 COMPARISION OF CALCULATED VALUE AND EXPERIMENATL RESULTS

The failure loads and stiffness for the same settings of the specimens are calculated, and the validity of the method is confirmed by comparing these calculations with the experimental results. Since the specimens are positioned vertically during the experiment, the experimental values are transformed for comparison as if the members were installed diagonally and subjected to horizontal loading like a unit model. In the same conditions as the unit model, let the horizontal load be P_H, the displacement be δ_H, and the stiffness be k_H. Similarly, in the experiment, let the horizontal load be P_E, the displacement be δ_E, and the stiffness be k_E. Then, the relationships of both situations are given by equation (18) to (20).

$$P_H = P_E / \sqrt{2} \tag{18}$$

$$\delta_H = \sqrt{2}\delta_E \tag{19}$$

$$k_H = P_H / \delta_H = P_E / (2\delta_E) \tag{20}$$

Fig. 14 shows the calculated failure loads for each test specimen using equation (10) to (13). Among the failure modes shown in Fig. 14, tensile failure resulted in the lowest failure load in linear member, and shear failure resulted in the lowest failure load in curbed members.

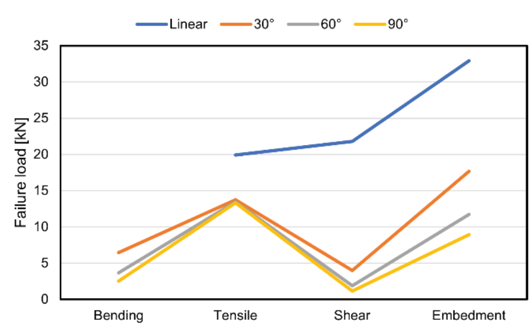

Figure 14. Calculated Failure Load

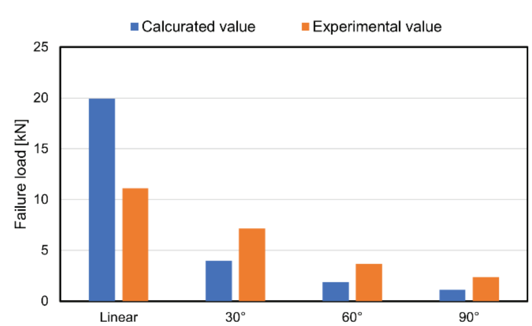

Figure 15. Comparison of Calculated Failure Load

https://doi.org/10.52202/080513-0236

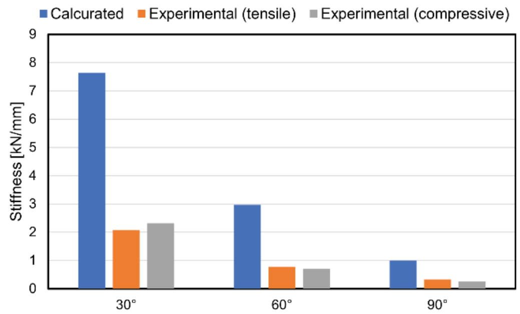

Figure 16. Comparison of Stiffness

Fig. 15 compares the calculated and experimental values of failure loads. The experimental failure load of the linear member was approximately half of the calculated ultimate load. As observed in Fig. 11-(a), a crack initiated from one side of the specimen and propagated toward the center. The failure occurred along the adhesive interface of the plywood layer where the central steel plate was embedded. These observations suggest that, in the experiment on the linear member, only half of the theoretically effective cross-section contributed to the structural capacity. On the other hand, for the curved member specimens, the experimental failure loads exceeded the calculated values. This indicates that the shear load equation may require revision.

Fig. 16 compares the calculated and experimental values of stiffness, and the calculated values exceeded the experimental results in all specimens. Equation (14) used in previous studies was developed for members composed of a single material. However, the specimens in this study consist of plywood, joints, and steel plates. The equation does not account for rotational deformation that may occur at the joints; therefore, the experimentally obtained stiffness was lower than the calculated value. Improving the stiffness equation remains a subject for future research.

6 – CONCLUSION

In this study, we aimed to improve the design method for wooden unit shear walls composed of curved members by considering geometric nonlinearity and details of the joints. We were able to obtain the load-deformation relationships for the plywood itself and for a unit of curved members. However, when comparing the experimental results and calculated value of the failure load and stiffness, it can be said that the theoretical models do not adequately represent the actual phenomena. Improving the accuracy of the theoretical equations and expanding the approach to multiple units are future challenges.

7 – REFERENCES

[1] M. Kitachi, Y. Shimada and S. Yoshitomi. "Performance based design method for unit load-bearing wall composed of curved members" In: Journal of Structural and Construction Engineering (Transactions of AIJ) 88.807 (2023), pp. 768-775

[2] Japan Wood Research Society. "Structural Timber Strength Testing Manual." Technical report. Japan Housing and Wood Technology Center, March 2011.

[3] Masahiro Inayama. "Guide for Structural Design of Medium to Large Wooden Buildings." Technical report. August 2019.

8 – APPENDIX

8.1 DERIVATION OF DEFORMATION WITH GEOMETRIC NONLINEARITY

The stress in the curved member is expressed as follows:

$$N(\theta) = -\sqrt{2}P\cos(\theta - \varphi/2) \tag{a.1}$$

$$Q(\theta) = -\sqrt{2}P\sin(\theta - \varphi/2) \tag{a.2}$$

$$M(\theta) = \sqrt{2}\,\Pr\left\{\cos(\theta - \varphi/2) - \cos(\varphi/2)\right\} \tag{a.3}$$

$$\overline{M(\theta)} = \begin{cases} \sqrt{2}r\sin\dfrac{\theta}{2}\sin\left(\dfrac{\theta}{2}+\alpha\right) & \left(0 < \theta < \dfrac{\varphi}{2}\right) \\ r\sin\dfrac{\varphi}{2} - \sqrt{2}r\sin\dfrac{\theta}{2}\cos\left(\dfrac{\theta}{2}+\alpha\right) & \left(\dfrac{\varphi}{2} < \theta < \varphi\right) \end{cases} \tag{a.4}$$

$$\alpha = \frac{\pi}{4} - \frac{\varphi}{2} \tag{a.5}$$

Let the Young's modulus of steel and wood be E_s and E_w [N/mm^2], and the section modulus be I_s and I_w [mm^4].

$$\begin{aligned} \delta_{s(1)} &= \int_0^{\theta_1} \frac{M(\theta)\overline{M(\theta)}}{E_s I_s} r\,d\theta + \int_{\varphi-\theta_1}^{\varphi} \frac{M(\theta)\overline{M(\theta)}}{E_s I_s} r\,d\theta \\ &= \frac{Pr^3}{2\sqrt{2}E_s I_s}\left\{\begin{matrix} -\sin(2\theta_1 - \varphi) + \cos(2\theta_1 - \varphi) \\ +4\sin(\theta_1 - \varphi) + 4\cos(\theta_1 - \varphi) + 4\sin\theta_1 \\ +4\theta_1 - (2\theta_1 - 3)\sin\varphi - (2\theta_1 + 3)\cos\varphi \end{matrix}\right\} \end{aligned} \tag{a.6}$$

$$\delta_{r(1)} = \frac{M(\theta_2)}{K_e r_{12}} = \frac{\sqrt{2}\,\Pr\left\{\cos(\theta_2 - \varphi/2) - \cos(\varphi/2)\right\}}{2K_e r\sin(\theta_2/2 - \theta_1/2)} \tag{a.7}$$

$$\delta_{w(1)} = \int_{\theta_2}^{\varphi} \frac{M(\theta)\overline{M(\theta)}}{E_w I_w} r d\theta$$

$$= \frac{Pr^3}{2\sqrt{2}E_w I_w} \left\{ \begin{array}{l} \sin(2\theta_2 - \varphi) - \cos(2\theta_2 - \varphi) \\ -4\sin(\theta_2 - \varphi) - 4\cos(\theta_2 - \varphi) + 4\sin\theta_2 \\ +4\theta_2 + (2\theta_2 + \varphi)\sin\varphi + (2\theta_2 - \varphi)\cos\varphi \\ +2\varphi\cos(\varphi/2) - 2\varphi + 1 \end{array} \right\} \tag{a.8}$$

$$\therefore \delta_{(1)} = \delta_{s(1)} + \delta_{r(1)} + \delta_{w(1)}$$

$$= \frac{Pr^3}{2\sqrt{2}E_s I_s} \left\{ \begin{array}{l} -\sin(2\theta_1 - \varphi) + \cos(2\theta_1 - \varphi) \\ +4\sin(\theta_1 - \varphi) + 4\cos(\theta_1 - \varphi) + 4\sin\theta_1 \\ +4\theta_1 - (2\theta_1 - 3)\sin\varphi - (2\theta_1 + 3)\cos\varphi \end{array} \right\}$$

$$+ \frac{\sqrt{2}\,\mathrm{Pr}\left\{\cos(\theta_2 - \varphi/2) - \cos(\varphi/2)\right\}}{2K_e r \sin(\theta_2/2 - \theta_1/2)}$$

$$+ \frac{Pr^3}{2\sqrt{2}E_w I_w} \left\{ \begin{array}{l} \sin(2\theta_2 - \varphi) - \cos(2\theta_2 - \varphi) \\ -4\sin(\theta_2 - \varphi) - 4\cos(\theta_2 - \varphi) + 4\sin\theta_2 \\ +4\theta_2 + (2\theta_2 + \varphi)\sin\varphi + (2\theta_2 - \varphi)\cos\varphi \\ +2\varphi\cos(\varphi/2) - 2\varphi + 1 \end{array} \right\} \tag{a.9}$$

In the same way, the additional moment generated by deformation is added to the bending moment, and perform the second iteration of deformation d_2. Deformations of steel plate, joint section, and plywood are expressed as $\delta_{s(2)}$, $\delta_{r(2)}$, and $\delta_{w(2)}$, respectively.

$$M(\theta) = \sqrt{2}Pr\left\{\cos(\theta - \varphi/2) - \cos(\varphi/2)\right\} + \sqrt{2}P\delta_1 \tag{a.10}$$

$$\delta_{s(2)} = \int_0^{\theta_1} \frac{M(\theta)\overline{M(\theta)}}{E_s I_s} r d\theta + \int_{\varphi - \theta_1}^{\varphi} \frac{M(\theta)\overline{M(\theta)}}{E_s I_s} r d\theta$$

$$= \delta_{s(1)} + \frac{\sqrt{2}Pr^2\delta_{(1)}}{E_s I_s} \left\{ \begin{array}{l} -\sin(\theta_1 - \varphi/2) + \cos(\theta_1 - \varphi/2) \\ +(\theta_1 - 1)\sin(\varphi/2) + (\theta_1 + 1)\cos(\varphi/2) \end{array} \right\} \tag{a.11}$$

$$\delta_{r(2)} = \frac{M(\theta_2)}{K_e r_{12}} = \delta_{r(1)} + \frac{\sqrt{2}P\delta_{(1)}}{2K_e r \sin(\theta_2/2 - \theta_1/2)} \tag{a.12}$$

$$\delta_{w(2)} = \int_{\theta_2}^{\varphi} \frac{M(\theta)\overline{M(\theta)}}{E_w I_w} r d\theta$$

$$= \delta_{w(1)} + \frac{\sqrt{2}Pr^2\delta_{(1)}}{E_w I_w} \left\{ \begin{array}{l} \sin(\theta_2 - \varphi/2) + \cos(\theta_2 - \varphi/2) \\ -(\theta_2 - \varphi/2)\sin(\varphi/2) \\ -(\theta_2 - \varphi/2)\cos(\varphi/2) - 1 \end{array} \right\} \tag{a.13}$$

$$\delta_{(2)} = \delta_{s(2)} + \delta_{r(2)} + \delta_{w(2)} = (1 + c)c\delta_{(1)} \tag{a.14}$$

$$c = \frac{\sqrt{2}Pr^2}{E_s I_s} \left\{ \begin{array}{l} -\sin(\theta_1 - \varphi/2) + \cos(\theta_1 - \varphi/2) \\ +(\theta_1 - 1)\sin(\varphi/2) + (\theta_1 + 1)\cos(\varphi/2) \end{array} \right\}$$

$$+ \frac{\sqrt{2}P}{2K_e r \sin(\theta_2/2 - \theta_1/2)}$$

$$+ \frac{\sqrt{2}Pr^2}{E_w I_w} \left\{ \begin{array}{l} \sin(\theta_2 - \varphi/2) + \cos(\theta_2 - \varphi/2) \\ -\theta_2\sin(\varphi/2) - \theta_2\cos(\varphi/2) \\ +\varphi\sin(\varphi/2)/2 + \varphi\cos(\varphi/2)/2 - 1 \end{array} \right\} \tag{a.15}$$

By repeating this calculation process, the deformation at the n-th step of the iterative calculation d_n can be expressed as the sum of a geometric series with the first term d_1 and a common ratio c.

$$\delta_{(n)} = (1 - c^n)\delta_{(1)} \big/ (1 - c) \tag{a.16}$$

From the above, the deformation as n approaches infinity can be expressed as follows, using c ($0<c<1$)).

$$\delta_{(\infty)} = \lim_{n\to\infty}\delta_{(n)} = \delta_{(1)} \big/ (1 - c) \tag{a.17}$$

Then the deformation at the position of angle q is expressed as a ratio relative to the value at the central position (q=j/2).

$$\delta_{(\infty)}(\theta) = \frac{\left\{\cos(\theta - \varphi/2) - \cos(\varphi/2)\right\}}{1 - \cos(\varphi/2)}\delta_{(\infty)} \tag{a.18}$$

Also, the bending moment considering nonlinearity is expressed as follows.

$$M(\theta) = \sqrt{2}Pr\left\{\cos(\theta - \varphi/2) - \cos(\varphi/2)\right\} + \sqrt{2}P\delta_{(\infty)}(\theta) \tag{a.19}$$

8.2 DERIVING HORIZONTAL LOADS FROM EACH FAILURE TYPE

The horizontal loads at which maximum edge stress s(j/2) [N], tensile failure P_t [N], shear failure P_s [N], and embedment failure P_e [N] occur in the curved member are calculated as follows;

$$\sigma(\varphi/2) = F_b = \left|M(\varphi/2)\right| \big/ Z + \left|N(\varphi/2)\right| \big/ A$$
$$= \left|\sqrt{2}Pr\left\{\cos(\theta - \varphi/2) - \cos(\varphi/2)\right\} + \sqrt{2}P\delta_\infty\right| \big/ Z$$
$$+ \left|-\sqrt{2}P\cos(\theta - \varphi/2)\right| \big/ A$$

https://doi.org/10.52202/080513-0236

(a.20)

$$\therefore P = \frac{F_b / \sqrt{2}}{\frac{\left| r\left\{\cos\left(\theta - \varphi/2\right) - \cos\left(\varphi/2\right)\right\} + \delta_\infty \right|}{Z} + \frac{\left|\cos\left(\theta - \varphi/2\right)\right|}{A}}$$

(a.21)

$$P_t = b\left(h-d\right)F_t = N\left(\theta_2\right) = \sqrt{2}P\cos\left(\theta - \varphi/2\right) \text{ (a.22)}$$

$$\therefore P = b\left(h-d\right)F_t \Big/ \left\{\sqrt{2}\cos\left(\theta - \varphi/2\right)\right\} \qquad \text{(a.23)}$$

$$\begin{aligned} P_s &= b\left(h-d\right)F_s = M\left(\theta_2\right)/r_{12} \\ &= \frac{\sqrt{2}Pr\left\{\cos\left(\theta_2 - \varphi/2\right) - \cos\left(\varphi/2\right)\right\} + \sqrt{2}P\delta_\infty\left(\theta_2\right)}{r\sin\left(\theta_2/2 - \theta_1/2\right)} \end{aligned}$$

(a.24)

$$\therefore P = \frac{b\left(h-d\right)F_s r\sin\left(\theta_2/2 - \theta_1/2\right) \Big/ \sqrt{2}}{r\left\{\cos\left(\theta_2 - \varphi/2\right) - \cos\left(\varphi/2\right)\right\} + \delta_\infty\left(\theta_2\right)}$$

(a.25)

$$\begin{aligned} P_e &= bdF_e = M\left(\theta_2\right)/r_{12} \\ &= \frac{\sqrt{2}Pr\left\{\cos\left(\theta_2 - \varphi/2\right) - \cos\left(\varphi/2\right)\right\} + \sqrt{2}P\delta_\infty\left(\theta_2\right)}{r\sin\left(\theta_2/2 - \theta_1/2\right)} \end{aligned}$$

(a.26)

$$\therefore P = \frac{bdF_e r\sin\left(\theta_2/2 - \theta_1/2\right) \Big/ \sqrt{2}}{r\left\{\cos\left(\theta_2 - \varphi/2\right) - \cos\left(\varphi/2\right)\right\} + \delta_\infty\left(\theta_2\right)} \quad \text{(a.27)}$$